

## ARTICLE

# Effect of Si content on the microstructure and properties of Al–Si alloys fabricated using hot extrusion

Pan Ma<sup>a)</sup>

*School of Materials Engineering, Shanghai University of Engineering Science, Shanghai 201620, China*

Yandong Jia

*Laboratory for Microstructures, Institute of Materials, Shanghai University, Shanghai 200444, China*

Konda Gokuidoss Prashanth<sup>b)</sup>

*Erich Schmid Institute of Materials Science, Austrian Academy of Sciences, A-8700 Leoben, Austria; and Norwegian University of Science and Technology, Gjøvik, Norway*

Zhishui Yu, Chonggui Li, Jian Zhao, Shanglei Yang, and Lixin Huang

*School of Materials Engineering, Shanghai University of Engineering Science, Shanghai 201620, China*

(Received 5 February 2017; accepted 3 March 2017)

Al–(12, 20, 35 wt%)Si alloys were fabricated using powder metallurgy process involving hot pressing followed by hot extrusion. The effect of Si content on the microstructure [by scanning electron microscopy], the mechanical properties (hardness and tensile tests), and the thermal expansion behavior were studied in detail, respectively. Due to the friction between the Si phase and the matrix, as well as the diffusion of the Si atoms, the Si phase becomes a particulate shape after hot extrusion, and the size increases with increasing Si content. The mechanical strength increases, whereas, the elongation decreases with increasing the Si content from 12 to 35 wt%, which lead to a variation of the fracture mechanism from ductile to brittle failure. The coefficient of thermal expansion (CTE) decreases with increasing Si content as a result of restriction of Si on the Al matrix, and the measured CTE value is in good agreement with the Turner model below 573 K.

## I. INTRODUCTION

Al–Si alloys, both hypoeutectic and hypereutectic grades, are known as typical high-strength, corrosion resistance, and light-weight materials, which makes them attractive for applications in automobile and aerospace industries.<sup>1–4</sup> The excellent mechanical and the physical properties of these alloys are attributed to hard Si particles embedded in an Al matrix.<sup>5–8</sup> It is known that the size and shape of Si particles in the Al–Si alloy play an important role in determining the properties, and fine Si particles are a necessary prerequisite to get desirable properties.<sup>7,9–13</sup>

The Al–Si alloys have been fabricated and investigated widely for decades; several fabrication techniques, such as stir casting,<sup>14</sup> squeeze casting,<sup>15,16</sup> spray forming,<sup>17,18</sup> powder metallurgy,<sup>19–21</sup> additive manufacturing via powder bed fusion processes,<sup>22–24</sup> can be applied to produce this alloy. The casting techniques offer low cost for production and high performance, however lack in flexibility and design. Nevertheless, some pores get entrapped during the solidification process due to the large size and irregular shape of the Si phase. In addition,

the Si content is difficult to control precisely during the casting process and also the morphology of the Si particles.<sup>25</sup> Lately, refiners/modifiers are used to control the morphology of the Si particles during the casting process.<sup>26,27</sup> The spray deposition method can also effectively decrease the size of the Si phase and can change the morphology of the Si phase. Since, it involves the use of inert gases like nitrogen during the atomization process, a small amount of nitrogen may be adsorbed at the surface of the powder, which may be detrimental during the consolidation process.<sup>28</sup> Even though solid state production costs are relatively higher than conventional casting processes, this alloy produced using solid state processes may exhibit excellent finished performances.<sup>29</sup> Powder metallurgy (PM) followed by sintering or extrusion is a common solid state manufacturing technique, which offers low sintering temperature, near net-shape formability, high productivity, as well as high relative density, and it is possible to use the processes efficiently.<sup>30</sup> Additive manufacturing is another option to process these alloys; however, it becomes expensive, if large batches of alloys are to be processed.<sup>31</sup>

In this study, both hypoeutectic and hypereutectic Al–Si alloys were fabricated by the powder metallurgy process using hot pressing followed by hot extrusion. The effect of Si morphology (size, shape, and distribution) on the mechanical properties and the thermal expansion

Contributing Editor: Jürgen Eckert

Address all correspondence to these authors.

<sup>a)</sup>e-mail: mapanhit@hotmail.com

<sup>b)</sup>e-mail: kgprashanth@gmail.com

DOI: 10.1557/jmr.2017.97

behavior is investigated in detail followed by fracture mechanism studies.

## II. EXPERIMENTAL DETAILS

Al–Si gas atomized powder with three different compositions was used in this study. The composition of the powders is given in Table I. The powders were hot pressed at 673 K for 15 min under a protective argon gas atmosphere to form cylindrical compacts with a size of about  $\varphi 10 \times 10$  mm. Sintered compacts were then hot-extruded at 723 K with an extrusion ratio of 9:1. The pressures applied in hot pressing and hot extrusion are 500 MPa and 700 MPa, respectively.

Chemical analysis of the powders were conducted by LSM International using bead fusion and analysis on a wavelength dispersive X-ray fluorescence (XRF). The microstructure of the Al–Si alloys was characterized by a scanning electron microscope (SEM; Gemini 1530, Zeiss, Oberkochen, Germany). The samples for SEM observation

TABLE I. Compositions and oxygen contents of Al–Si gas atomic powders.

Norminal composition (wt%)	Chemical composition (wt%)	Oxygen content (wt%)
Al <sub>88</sub> Si <sub>12</sub>	Al <sub>86.62</sub> Si <sub>11.88</sub>	0.09 $\pm$ 0.01
Al <sub>80</sub> Si <sub>20</sub>	Al <sub>77.97</sub> Si <sub>18.58</sub>	0.14 $\pm$ 0.02
Al <sub>65</sub> Si <sub>35</sub>	Al <sub>63.5</sub> Si <sub>33.86</sub>	0.13 $\pm$ 0.02

were etched in 0.5 vol% HF solution (0.5 vol% HF + 99.5 vol% H<sub>2</sub>O) for 20 s. ImageJ software (National Institutes of Health, Wayne, Rasband) was adopted to calculate the average size of Si particles based on the SEM images. Structural characterization of the samples was studied using X-ray diffraction (XRD; X'Pert Pro Diffraction, PANalytical B.V., Almelo, The Netherlands; Cu K $\alpha$  radiation, reflection geometry). Archimedes' principle was used to evaluate the density of the samples.

The Vickers microhardness measurements were carried out at a load of 500 gf and were held for 15 s using a HV-1000Z-type digital microhardness tester (Jinan Kason Testing Equipment Co. Ltd., Jinan, China). Room temperature mechanical properties were performed on an Instron 5569 electronic universal testing machine (Fiedler Optoelektronik GmbH, Luetzen, Germany) at a strain rate of  $10^{-4}$  s<sup>-1</sup>. The tensile fracture morphology was studied using SEM. To ensure the reproducibility, at least six measurements were carried out at each condition.

Thermal expansion analysis was performed on a NETZSCH DIL 402C dilatometer (NETZSCH GmbH & Co., Selb, Germany) using heating and cooling rates of 5 K per minute from room temperature to 723 K under an argon atmosphere. To eliminate systematic errors, the dilatometer was calibrated by measuring a silica sample under the same experimental conditions. Each result presented here is an average of three distinct experiments. Cylindrical samples of 4 mm diameter and 25 mm length were used for the thermal expansion analysis measurements. The top and the

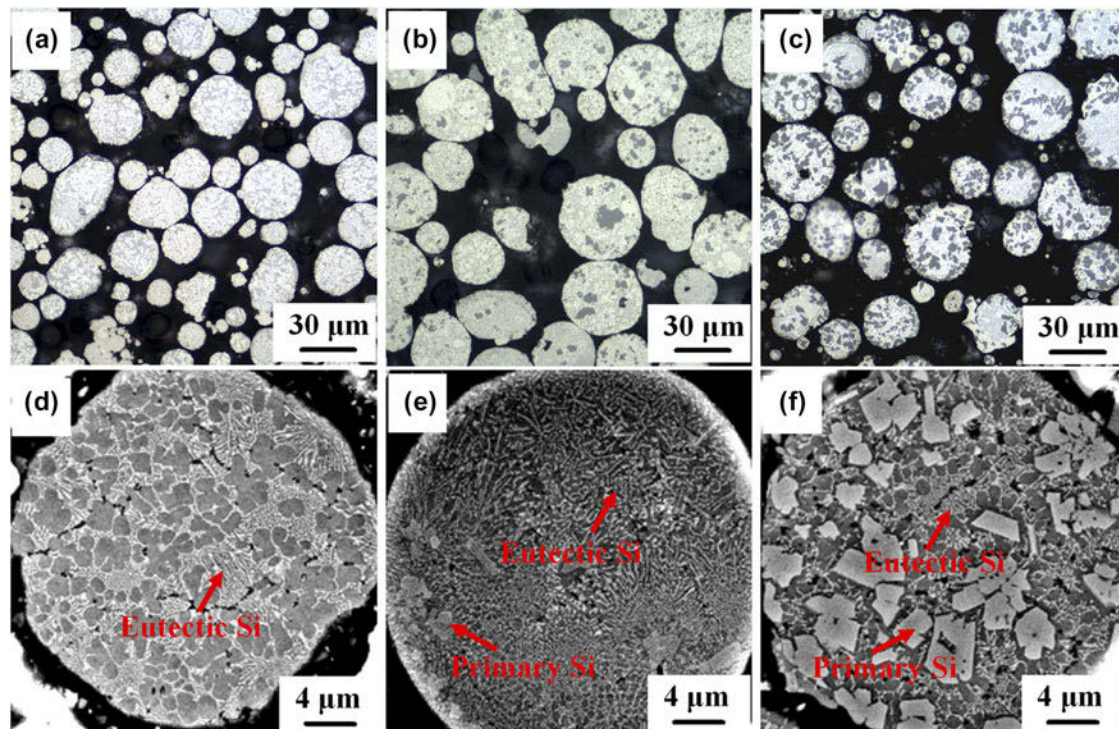


FIG. 1. Microstructures of (a, d) Al–12Si, (b, e) Al–20Si, (c, f) Al–35Si gas atomized powders.

bottom of the specimens were polished to guarantee plane-parallel surfaces.

### III. RESULTS AND DISCUSSION

#### A. Microstructure and phase composition of Al–Si alloys

The microstructures of the gas atomized powders are given in Fig. 1. As can be seen, most of the particles are spherical in shape, with their size ranging between 20 and 30  $\mu\text{m}$ . Eutectic Si and primary Si can be observed obviously in the microstructure. Moreover, the grain boundaries can also be found clearly and the grain size observed in these alloys were similar, which is  $\sim 8 \pm 0.5 \mu\text{m}$ .

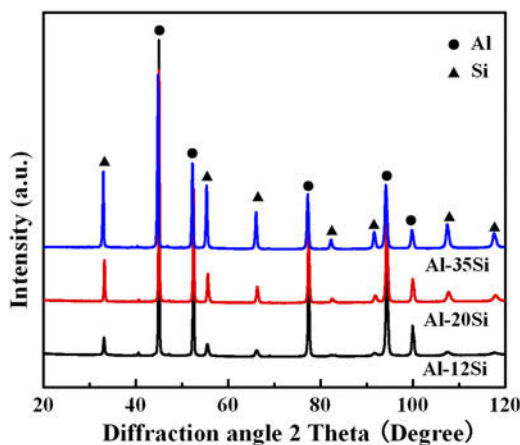


FIG. 2. XRD patterns of Al–Si alloys prepared with hot extrusion.

Figure 2 shows XRD patterns of the Al–Si alloys fabricated with hot extrusion. As expected, only  $\alpha$ -Al and Si reflections are visible. There are no distinct peaks of impurities like oxygen visible, since they are present in small amounts that are hard to detect by X-rays. As the Si content increases, the intensity of the Si diffraction peaks increases.

The microstructures of the three different Al–Si alloys are shown in Fig. 3. As it can be seen in the Al–12Si sample, the small particles of Si are evenly distributed in the Al matrix after hot pressing and hot extrusion. As the Al–Si alloy is composed of soft Al and hard Si, during the extrusion, the Al becomes softer, and the deformation becomes homogeneous; thus, the Si particles can be evenly distributed in the Al matrix. Eutectic Si in the Al–12Si alloy varies its morphology from a fibrous to particulate shape. Both eutectic Si and primary Si in Al–20Si are present in the form of small particles, and it is difficult to distinguish primary Si and eutectic Si after hot extrusion. Fibrous eutectic Si in the Al–35Si alloy also varies to a particulate shape. It has been reported that an elongated Si phase tends to fracture more frequently than a particulate shape as a result of the introduction of high levels of stress concentration. Si breaks and partially dissolves into the matrix during extrusion. This would result in outstanding fracture elongation values as well as good yield strength (YS).<sup>32</sup> In addition, the size of primary Si in the Al–35Si alloy does not change significantly, however, its morphology changes to an irregular shape.

During the hot pressing and subsequent hot extrusion process, eutectic Si breaks and changes to a spherical shape gradually. Meanwhile, due to the friction between

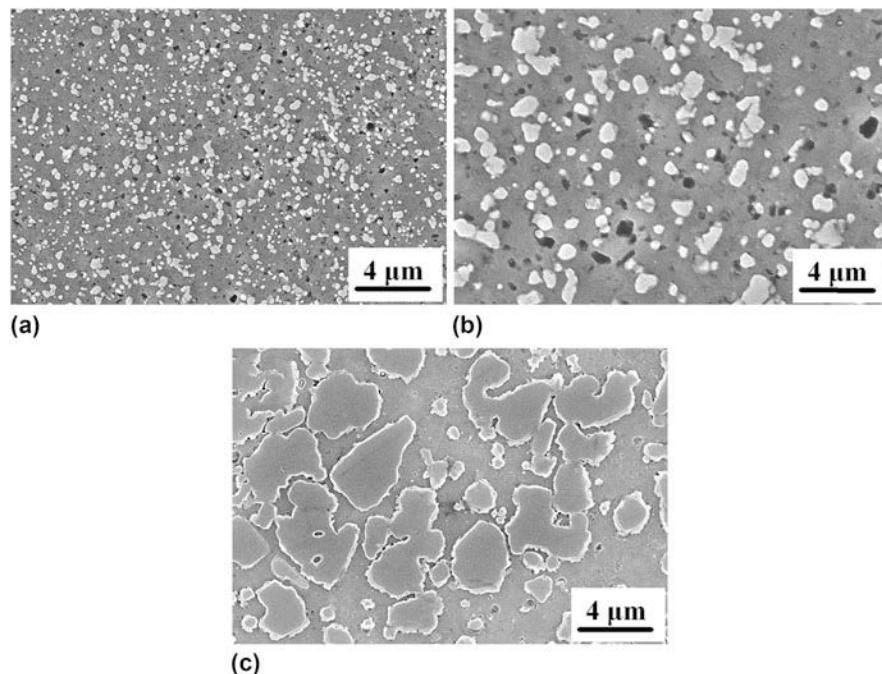


FIG. 3. SEM micrographs of Al–Si alloys after hot extrusion: (a) Al–12Si alloy, (b) Al–20Si alloy, and (c) Al–35Si alloy.

primary Si and the matrix, the edges of primary Si display a slight passivation. In addition, the diffusion of the Si atoms is also helpful for the passivation of the primary Si phase. Moreover, some Si particles grow in size due to diffusion aided by the hot pressing/extrusion conditions, mainly the thermal energy, as depicted in Fig. 3. The average sizes of the Si particles are found to be  $0.62 \pm 0.04 \mu\text{m}$ ,  $1.18 \pm 0.07 \mu\text{m}$ , and  $3.35 \pm 0.15 \mu\text{m}$  calculated to be in Al–12Si, Al–20Si, and Al–35Si alloys, respectively. The size of Si particles increases and its shape becomes more irregular with increasing the Si content.

The density and the relative density of the three different Al–Si alloys are measured and the results are demonstrated in Fig. 4. Due to the lower density of Si ( $\sim 2.3 \text{ g/cm}^3$ ) than Al ( $\sim 2.7 \text{ g/cm}^3$ ), the density of these alloys decreases with increasing Si content. In addition, the relative density decreases slightly with increasing Si content. With increasing Si content, the Si particles are observed to be larger in size leading to increased porosity levels at the interface between Al and Si in these samples as shown in Fig. 3.

## B. Mechanical properties of Al–Si alloys

The effect of the Si content on the mechanical properties is depicted in Fig. 5. Both the hardness and the tensile strength increase significantly with increasing

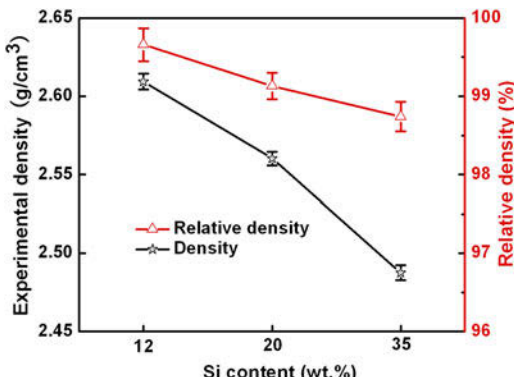


FIG. 4. Density of the Al–Si alloys consolidated by hot extrusion.

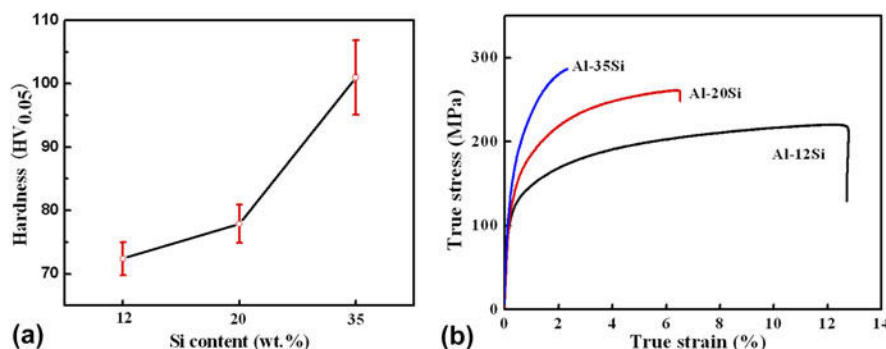


FIG. 5. Mechanical properties of the three different Al–Si alloys: (a) Hardness data, (b) tensile strain–stress curves.

Si content. The hardness values are found to be  $72.4 \pm 0.4 \text{ HV}_{0.05}$ ,  $77.9 \pm 0.5 \text{ HV}_{0.05}$ , and  $101 \pm 0.7 \text{ HV}_{0.05}$  for Al–12Si, Al–20Si, and Al–35Si alloys, respectively. The tensile property results are demonstrated in Table II in the form of true stress–strain curves. As observed, the ultimate tensile strength (UTS) and the YS of these alloys increase with increasing Si content, whereas the elongation shows an adverse trend. Published reports on powder metallurgy processed Al–Si alloys show UTSS of 148 MPa for Al–22Si and 196 MPa for Al–50Si alloys (fabricated by hot pressing).<sup>33</sup> Hence, the results observed here show improved mechanical properties, even though the comparison may not be fair, since the reported results consolidate the Al–Si samples by hot pressing and the present samples are consolidated by hot pressing and subsequent hot extrusion processes.

Figure 6 shows the fracture surfaces of Al–Si alloys after tensile tests. They exhibit the presence of large amounts of dimples and shapes in the Al–12Si alloy, indicating that the failure is the result of ductile fracture. As a result, all the tested Al–12Si samples exhibit better elongation. The dimples become larger in the Al–20Si alloy and some cleavage can be found in the fracture surfaces, which indicates the presence of both ductile and brittle modes of fracture. Whereas, in Al–35Si samples apart from dimples and cleavage surfaces, some cracks are also observed, as marked in Fig. 6(f), which indicates that the failure of the sample is predominantly by a brittle fracture mode. As a hard phase, the Si particles play a key role in the strengthening of the Al–Si alloy. The tensile loading generates stresses in the Al–Si samples, where Al as a soft phase deforms readily than hard Si. Consequently, a number of dislocation sources can be excited and started up within the matrix. When the dislocations

TABLE II. Tensile properties of Al–Si alloys after hot extrusion.

Alloy	UTS (MPa)	YS (MPa)	$\delta$ (%)
Al–12Si	$219.8 \pm 1.8$	$127.5 \pm 1.1$	$12.1 \pm 0.8$
Al–20Si	$261.5 \pm 2.1$	$173.2 \pm 1.5$	$5.8 \pm 0.1$
Al–35Si	$287.5 \pm 2.7$	$199.4 \pm 1.6$	$1.2 \pm 0.1$

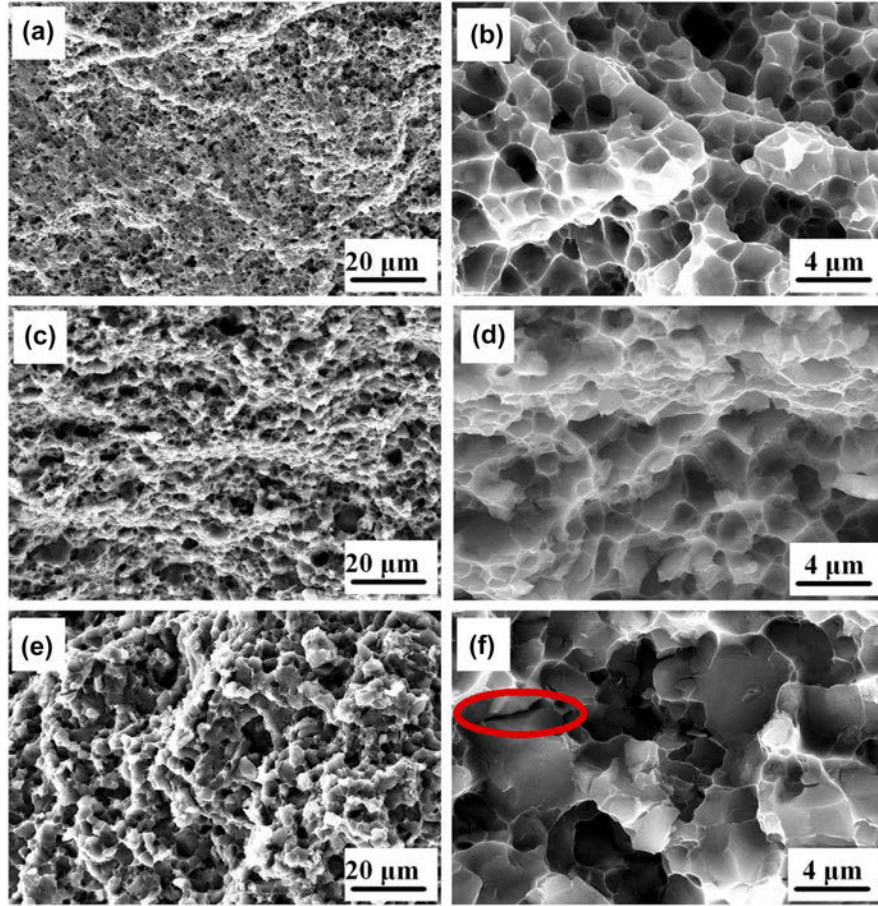


FIG. 6. Fracture surfaces of Al–Si alloys after hot pressing and subsequent hot extrusion: (a, b) Al–12Si alloy, (c, d) Al–20Si alloy, and (e, f) Al–35Si alloy.

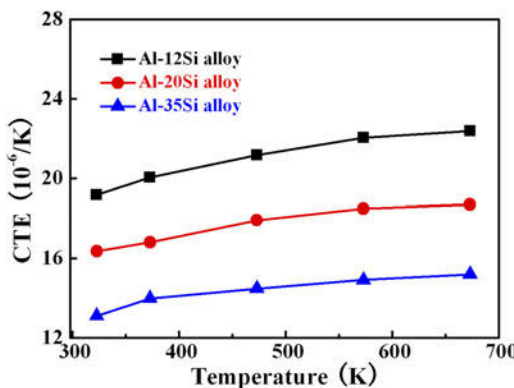


FIG. 7. CTEs of the three different Al–Si alloys after hot extrusion.

move and reach the Al/Si interfaces, the dislocations' pileup may take place due to the hindrance of the Si particles, which can effectively reduce the movement of dislocations. A relatively high stress must be applied to move the dislocation overcoming the obstacle which deforms it plastically. This maybe the main reason for improving the strength of the Al–35Si alloy. As it can be

TABLE III. Physical properties of Al and Si.<sup>17,40</sup>

	T (K)	323	373	473	573	673
Al	E (GPa)	69.2	67.6	64.0	59.8	54.9
	G (GPa)	26.0	25.4	24.1	22.3	20.2
	K (GPa)	67.8	66.3	62.7	62.3	65.4
	$\alpha$ ( $10^{-6}/\text{K}$ )	22.6	24.2	25.7	27.7	30.4
Si	E (GPa)	163	162	161	160	156
	G (GPa)	66.8	66.4	66.0	65.6	63.9
	K (GPa)	97.0	96.4	95.8	95.2	92.9
	$\alpha$ ( $10^{-6}/\text{K}$ )	2.5	3.0	3.4	3.6	3.8

observed in Fig. 6(f), the Al–35Si alloy cracks at the interface between Al and Si, which triggers the failure. Due to the irregular shape of Si particles, the stress normally segregates at the corners of the Si phase and can lead to premature crack initiation, deteriorating the overall mechanical properties of the alloy.

### C. Thermal expansion behavior of Al–Si alloys

The variation in the CTEs as a function of temperature for the Al–Si alloys is shown in Fig. 7. The CTEs of all

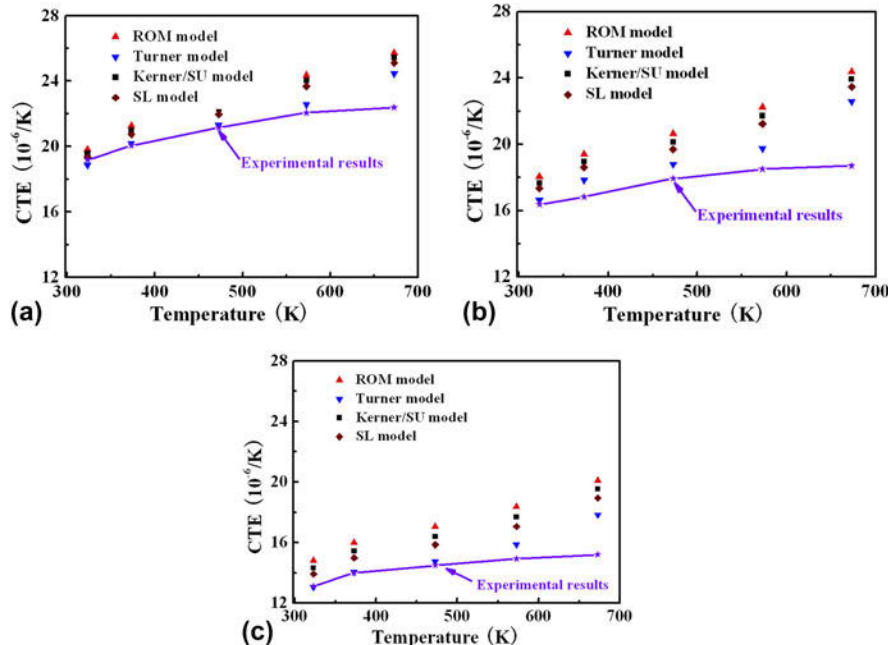


FIG. 8. Comparison between theoretical and experimental CTEs for the three different Al–Si alloys: (a) Al–12Si alloy, (b) Al–20Si alloy, and (c) Al–35Si alloy.

the alloys monotonically increase with increasing temperature. The CTEs of the sample with a high Si content show lower values compared with the ones with a low Si content. The coefficient of thermal expansion (CTE) decreases with increasing Si content. On the one hand, this can be attributed to the low CTE of Si particles. On the other hand, a high volume fraction of Si particles have a larger total specific surface area than that of the low content of Si in the Al–Si matrix, leading to a more effective restriction on the thermal expansion of Al in the matrix. Thus, the CTE of the alloy with more Si is lower than that with less ones, and its value decreases from  $19.2 \times 10^{-6}/\text{K}$  for the Al–12Si alloy to  $13.1 \times 10^{-6}/\text{K}$  for the Al–35Si alloy at room temperature. Moreover, compared with the CTE of Al–Si alloys fabricated by hot pressing,<sup>33</sup> this study displays a lower value as a result of the small size of the Si particles. The decreased size of the Si particles contributes to more Si/Al interfaces after hot extrusion, which can effectively inhibit the expansion of the Al matrix.

Several models are applied to calculate the effective CTE of alloys, such as the linear rule of mixtures (ROM),<sup>34,35</sup> the Turner model,<sup>36,37</sup> the Kerner model,<sup>37,38</sup> and the Schapery's model.<sup>38</sup> All the models are based on different assumptions as depicted in our previous work,<sup>39</sup> and some physical properties of Al and Si are given in Table III.

Figure 8 shows the comparison between theoretical and experimental CTEs for the three different Al–Si alloys. It can be found that all the experimental CTEs agree well with the Turner model at temperatures lower

than 573 K, but deviate from the other theoretical values. This can be ascribed to the small size of the Si phase after hot extrusion and well bonding between the Si phase and Al matrix. However, the experimental CTEs are lower than the Turner model when the temperature is higher than 573 K, which is caused by the increased solid solubility of Si in the Al matrix at elevated temperatures.

#### IV. CONCLUSIONS

In this study, by means of hot pressing and hot extrusion, Al–Si alloys with three different Si contents (12, 20, and 35 wt%) were manufactured and evaluated. Considering the results achieved, it is concluded that

(1) Al–Si alloys containing three different Si contents were fabricated using hot pressing and subsequent hot extrusion with relatively high densities. Si particles are homogeneously distributed in the Al matrix. The sizes of the Si particles in Al–12Si, Al–20Si, and Al–35Si are 0.62, 1.18, and 3.45  $\mu\text{m}$ , respectively.

(2) Both the UTS and YS increase with increasing the Si content from 219.8 MPa, 127.5 MPa in the Al–12Si alloy to 287.5 MPa, 199.4 MPa in the Al–35Si alloy, whereas the elongation exhibits an opposite trend. The fracture surfaces vary significantly. It shows a ductile fracture mode in the Al–12Si alloy, turns to be a mixture of ductile and brittle in the Al–20Si alloy, and finally changes to brittle fracture in the Al–35Si alloy.

(3) The CTE decreases with increasing Si contents. And its value decreases from  $19.2 \times 10^{-6}/\text{K}$  for the Al–12Si alloy to  $13.1 \times 10^{-6}/\text{K}$  for the Al–35Si alloy at

room temperature. The Turner model could be used to predict the CTE of the alloys for temperatures less than 573 K.

## ACKNOWLEDGMENTS

This project was supported by the National Key Research and Development Program of China (2016YFB0700203), the National Natural Science Foundation of China (Nos. 51601110, 51601109, 51375294, 51402189), the China Postdoctoral Science Foundation (No. 2016M601563), the Natural Science Foundation of Shanghai (No. 17ZR1440800, 14ZR1418300), the Youth Teacher Development Program of Shanghai Universities (Nos. ZZGCD15100, ZZGCD15036).

## REFERENCES

- G. Chirita, I. Stefanescu, D. Soares, and F.S. Silva: Influence of vibration on the solidification behaviour and tensile properties of an Al–18 wt% Si alloy. *Mater. Des.* **30**, 1575 (2009).
- R.J. Immanuel and S.K. Panigrahi: Influence of cryorolling on microstructure and mechanical properties of a cast hypoeutectic Al–Si alloy. *Mater. Sci. Eng., A* **640**, 424 (2015).
- S.P. Nikanorov, M.P. Volkov, V.N. Gurin, Y.A. Burenkov, L.I. Derkachenko, B.K. Kardashev, L.L. Regel, and W.R. Wilcox: Structural and mechanical properties of Al–Si alloys obtained by fast cooling of a levitated melt. *Mater. Sci. Eng., A* **390**, 63 (2005).
- Z. Cai, R. Wang, C. Zhang, C. Peng, and L. Wang: Microstructure and properties of Al/Si<sub>p</sub> composites for thermal management applications. *J. Mater. Sci.: Mater. Electron.* **26**, 4234 (2015).
- S.C. Hogg, A. Lambourne, A. Ogilvy, and P.S. Grant: Microstructural characterisation of spray formed Si–30Al for thermal management applications. *Scr. Mater.* **55**, 111 (2006).
- Z. Cai, R. Wang, C. Zhang, C. Peng, Y. Feng, and L. Wang: Thermal cycling reliability of Al/50Si<sub>p</sub> composite for thermal management in electronic packaging. *J. Mater. Sci.: Mater. Electron.* **26**, 4894 (2015).
- K.G. Prashanth, S. Scudino, H.J. Klauss, K.B. Surreddi, L. Löber, Z. Wang, A.K. Chaubey, U. Kühn, and J. Eckert: Microstructure and mechanical properties of Al–12Si produced by selective laser melting: Effect of heat treatment. *Mater. Sci. Eng., A* **590**, 153 (2014).
- P. Ma, K.G. Prashanth, S. Scudino, Y.D. Jia, H.W. Wang, C.M. Zou, Z.J. Wei, and J. Eckert: Influence of annealing on mechanical properties of Al–20Si processed by selective laser melting. *Metals* **1**, 28 (2014).
- Y. Birol: Grain refinement of pure aluminium and Al–7Si with Al–3B master alloy. *Mater. Sci. Technol.* **28**, 363 (2012).
- S.A. Kori, B.S. Murty, and M. Chakraborty: Development of an efficient grain refiner for Al–7Si alloy and its modification with strontium. *Mater. Sci. Eng., A* **283**, 94 (2000).
- Q.L. Li, T.D. Xia, Y.F. Lan, W.J. Zhao, L. Fan, and P.F. Li: Effect of rare earth cerium addition on the microstructure and tensile properties of hypereutectic Al–20% Si alloy. *J. Alloys Compd.* **562**, 25 (2013).
- C.L. Xu and Q.C. Jiang: Morphologies of primary silicon in hypereutectic Al–Si alloys with melt overheating temperature and cooling rate. *Mater. Sci. Eng., A* **437**, 451 (2006).
- K.G. Prashanth, S. Scudino, and J. Eckert: Defining the tensile properties of Al–12Si parts produced by selective laser melting. *Acta Mater.* **126**, 25 (2017).
- A.G. Rao, B.R.K. Rao, V.P. Deshmukh, A.K. Shah, and B.P. Kashyap: Microstructural refinement of a cast hypereutectic Al–30Si alloy by friction stir processing. *Mater. Lett.* **63**, 2628 (2009).
- W. Yu and J.K. Yu: Silicon dissolution and interfacial characteristics in Si/Al composites fabricated by gas pressure infiltration. *Mater. Chem. Phys.* **139**, 783 (2013).
- Y. Chen and D.D. Chung: Silicon–aluminum network composites fabricated by liquid metal infiltration. *J. Mater. Sci.* **29**, 6069 (1994).
- Y.D. Jia, F.Y. Cao, S. Scudino, P. Ma, H.C. Li, L. Yu, J. Eckert, and J.F. Sun: Microstructure and thermal expansion behavior of spray-deposited Al–50Si. *Mater. Des.* **57**, 585 (2014).
- C. Cui, A. Schulz, K. Schimanski, and H.W. Zoch: Spray forming of hypereutectic Al–Si alloys. *J. Mater. Process. Technol.* **209**, 5220 (2009).
- Y.Q. Liu, S.H. Wei, J.Z. Fan, Z.L. Ma, and T. Zuo: Mechanical properties of a low-thermal expansion aluminum/silicon composite produced by powder metallurgy. *J. Mater. Sci. Technol.* **30**, 417 (2014).
- H. Neubing, J. Gradl, and H. Danninger: Sintering and microstructure of Al–Si P/M components. *Adv. Powder Metall. Part. Mater.* **13**, 13 (2002).
- Z. Wang, K.G. Prashanth, A.K. Chaubey, L. Löber, F.P. Schmansky, F. Pyczak, W.W. Zhang, S. Scudino, and J. Eckert: Tensile properties of Al–12Si matrix composites reinforced with Ti–Al based particles. *J. Alloys Compd.* **630**, 256 (2015).
- K.G. Prashanth, B. Debalina, Z. Wang, P.F. Gostin, A. Gebert, M. Calin, U. Kühn, M. Kamaraj, S. Scudino, and J. Eckert: Tribological and corrosion properties of Al–12Si produced by selective laser melting. *J. Mater. Res.* **29**, 2044 (2014).
- J. Suryawanshi, K.G. Prashanth, S. Scudino, J. Eckert, O. Prakash, and U. Ramamurthy: Simultaneous enhancements of strength and toughness in an Al–12Si alloys synthesized using selective laser melting. *Acta Mater.* **115**, 285 (2016).
- K.G. Prashanth, R. Damodaram, S. Scudino, Z. Wang, K. Prasad Rao, and J. Eckert: Friction welding of Al–12Si parts produced by selective laser melting. *Mater. Des.* **57**, 632 (2014).
- L. Liu, A.M. Samuel, F.H. Samuel, H.W. Doty, and S. Valtierra: Influence of oxides on porosity formation in Sr-treated Al–Si casting alloys. *J. Mater. Sci.* **38**, 1255 (2003).
- X.R. Liu, Y.D. Zhang, B. Beausir, F. Liu, C. Esling, F.X. Yu, X. Zhao, and L. Zuo: Twin-controlled growth of eutectic Si in unmodified and Sr-modified Al–12.7% Si alloys investigated by SEM/EBSD. *Acta Mater.* **97**, 338 (2015).
- F.X. Guo, W. Wang, W.H. Yu, Y. Zhang, S.P. Pan, Z.H. Zhou, D. Liu, J.Y. Qin, Y. Wang, and X.L. Tian: Enhanced nucleation and refinement of eutectic Si by high number-density nanoparticles in Al–10Si–0.5Sb alloys. *Mater. Des.* **117**, 382 (2017).
- S.X. Ji, W.C. Yang, F. Gao, D. Watson, and Z.Y. Fan: Effect of iron on the microstructure and mechanical property of Al–Mg–Si–Mn and Al–Mg–Si die cast alloys. *Mater. Sci. Eng., A* **564**, 130 (2013).
- Y.D. Jia, F.Y. Cao, P. Ma, S. Scudino, J. Eckert, J.F. Sun, and G. Wang: Microstructure and thermal conductivity of hypereutectic Al–high Si produced by casting and spray deposition. *J. Mater. Res.* **31**, 2948 (2016).
- F. Bedir: Characteristic properties of Al–Cu–SiC<sub>p</sub> and Al–Cu–B<sub>4</sub>C<sub>p</sub> composites produced by hot pressing method under nitrogen atmosphere. *Mater. Des.* **28**, 1238 (2007).
- K.G. Prashanth, L. Löber, H-J. Klauss, U. Kühn, and J. Eckert: Characterization of 316L steel cellular dodecahedron structures produced by selective laser melting. *Technologies* **4**, 34 (2016).

32. B. Li, H.W. Wang, J.C. Jie, and Z.J. Wei: Effect of yttrium and heat treatment on the microstructure and tensile properties of Al–7.5Si–0.5Mg alloy. *Mater. Des.* **32**, 1617 (2011).
33. Z.Y. Cai, C. Zhang, R.C. Wang, C.Q. Peng, K. Qiu, and Y. Feng: Preparation of Al–Si alloys by a rapid solidification and powder metallurgy route. *Mater. Des.* **87**, 996 (2015).
34. S. Elomari, M.D. Skibo, A. Sundarrajan, and H. Richards: Thermal expansion behaviour of particulate metal-matrix composites. *Compos. Sci. Technol.* **58**, 369 (1998).
35. W.A. Uju and I.N.A. Oguocha: A study of thermal expansion of Al–Mg alloy composites containing fly ash. *Mater. Des.* **33**, 503 (2012).
36. S. Nagarajan, B. Dutta, and M.K. Surappa: The effect of SiC particles on the size and morphology of eutectic silicon in cast A356/SiC<sub>p</sub> composites. *Compos. Sci. Technol.* **59**, 897 (1999).
37. N. Chawla, X. Deng, and D.R.M. Schnell: Thermal expansion anisotropy in extruded SiC particle reinforced 2080 aluminum alloy matrix composites. *Mater. Sci. Eng., A* **426**, 314 (2006).
38. Z. Hashin and S. Shtrikman: A variational approach to the elastic behavior of multiphase materials. *J. Mech. Phys. Solids* **11**, 127 (1963).
39. Z.J. Wei, P. Ma, H.W. Wang, C.M. Zou, S. Scudino, K.K. Song, K.G. Prashanth, W. Jiang, and J. Eckert: The thermal expansion behaviour of SiC<sub>p</sub>/Al–20Si composites solidified under high pressures. *Mater. Des.* **65**, 387 (2015).
40. T. Huber, H.P. Degischer, G. Lefran, and T. Schmitt: Thermal expansion studies on aluminium-matrix composites with different reinforcement architecture of SiC particles. *Compos. Sci. Technol.* **66**, 2206 (2006).